Supplementary Information

Flexible SiO_2 Nanofilms Assembled on Poly(ethylene terephthalate) Substrates through a Room Temperature Fabrication Process for Nanoscale Integration

Shunsuke Yamamoto, Kazuki Sonobe, Tokuji Miyashita, Masaya Mitsuishi*

Details for Polymer Synthesis

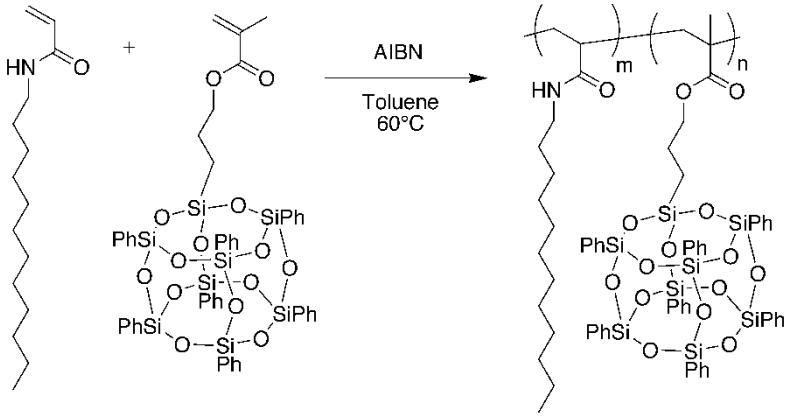

Figure S1. Reaction scheme of polymerization reaction for p(DDA/SQ22).

Copolymer was obtained by free radical polymerization in anhydrous toluene (Wako Pure Chemical Inds. Ltd.) using azobisisobutyronitrile (AIBN) as initiator. Monomers and AIBN were purified by recrystallization from chloroform/hexane mixture and methanol, respectively. The solution of DDA (252 mg, 1.05 mmol), MMA-$SQPh_7$ (486 mg, 0.45 mmol), and AIBN (1.82 mg, 0.01 mmol) in toluene (20 mL) was degassed using freeze–pump–thaw cycles for five times before the polymerization reaction at 60 °C for 32 h. The resulting solution was concentrated and poured into acetonitrile (Kanto Chemical Co. Inc.) for reprecipitation. The obtained polymer was reprecipitated two more times, and was then allowed to dry in vacuum overnight. p(DDA/SQ) (244 mg, 33%) was obtained as white powder. The molecular weight of this polymer was estimated by SEC measurement with polystyrene standard to be $M_n = 1.2 \times 10^4$ and $M_w = 2.7 \times 10^4$. It is noteworthy that ^{29}Si-NMR

signal has two peaks at around −78 ppm, which is characteristic to silsesquioxane structure ($RSiO_{1.5}$) even after the polymerization reaction, which indicates that the silsesquioxane cage is not deformed during the polymerization reaction. ^{1}H NMR (400.1 MHz, $CDCl_3$) δ 0.86, 1.25, 1.45, 1.79, 2.00, 3.13, 3.87, 6.36, 7.33, 7.72 ppm; ^{13}C NMR (100.6 MHz, $CDCl_3$) δ 14.1, 22.7, 29.7, 32.0, 127.9, 134.2 ppm; ^{29}Si NMR (99.4 MHz, $CDCl_3$ with $Cr(acac)_3$) δ −77.7, −78.0 ppm; elemental analysis C 63.4%, H 8.34%, N 2.98%.

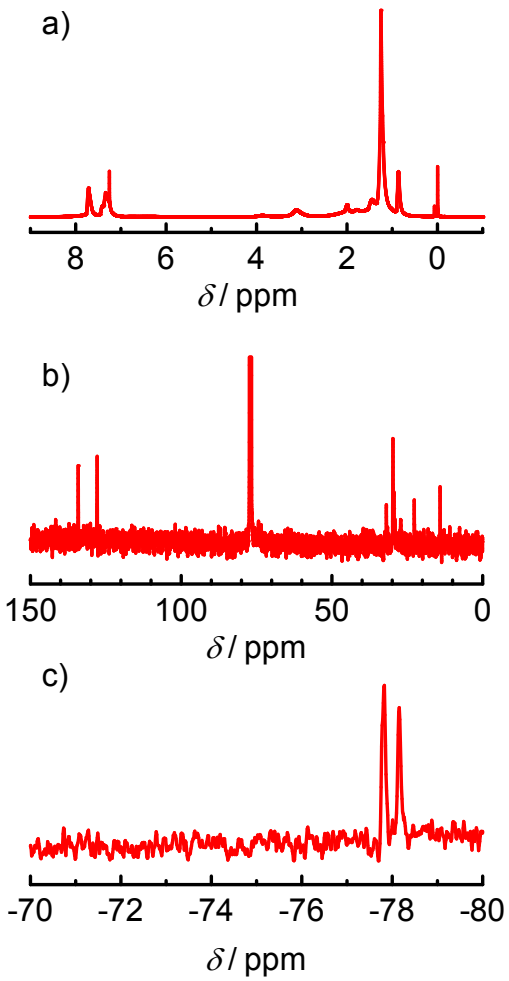

Figure S2. ^{1}H, ^{13}C, and ^{29}Si NMR spectra of p(DDA/SQ22) in $CDCl_3$ solution.

Monolayer Behavior of p(DDA/SQ22)

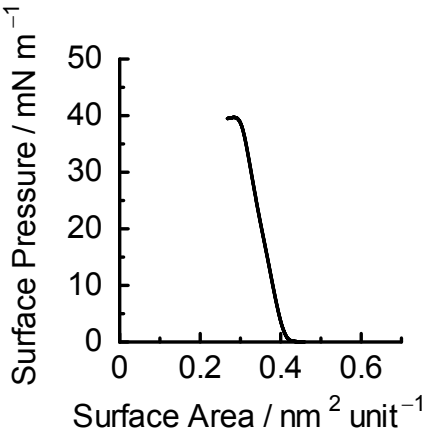

Figure S3. π-A isotherm of p(DDA/SQ22) monolayer at the air–water interface measured at 20 °C.

UV–Vis Absorption Spectra of p(DDA/SQ22) LB Films

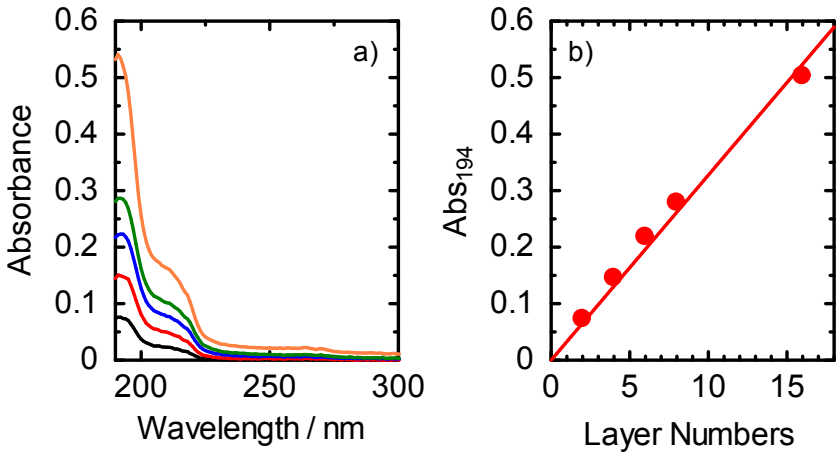

Figure S4. (a) UV–Vis absorption spectra of p(DDA/SQ22) LB films on quartz substrates. (b) plot of absorbance at 194 nm against the number of layers. Solid line shows linear fitting for data.

AFM Image of Films

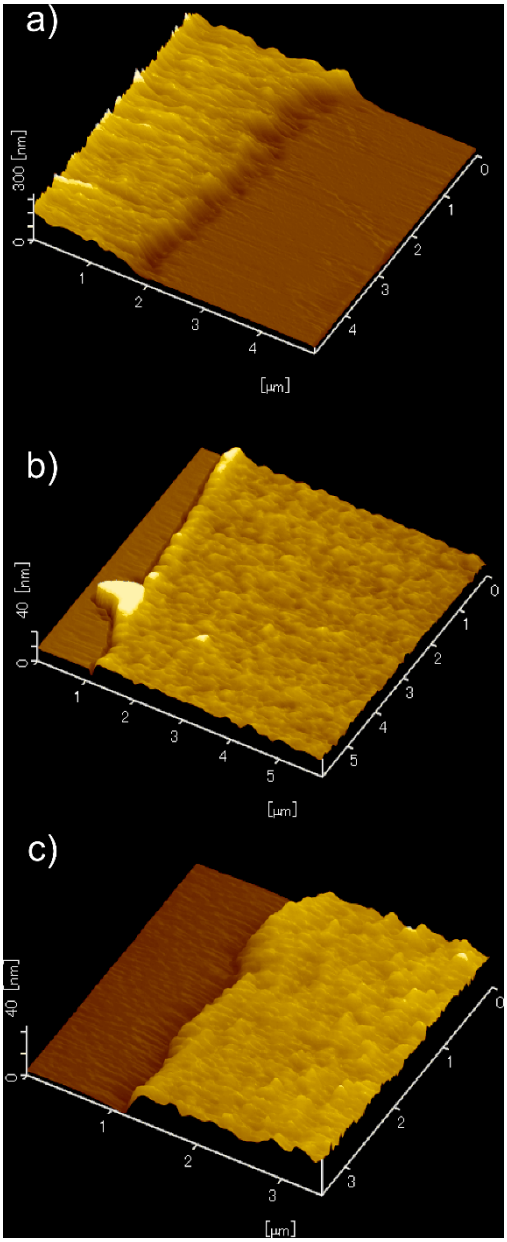

Figure S5. AFM images of p(DDA/SQ22) LB films with (a, b) 20 and (c) 40 layers (a) before and (b, c) after photo-oxidization.

XPS spectra of the original and photo-oxidized p(DDA/SQ22) LB films

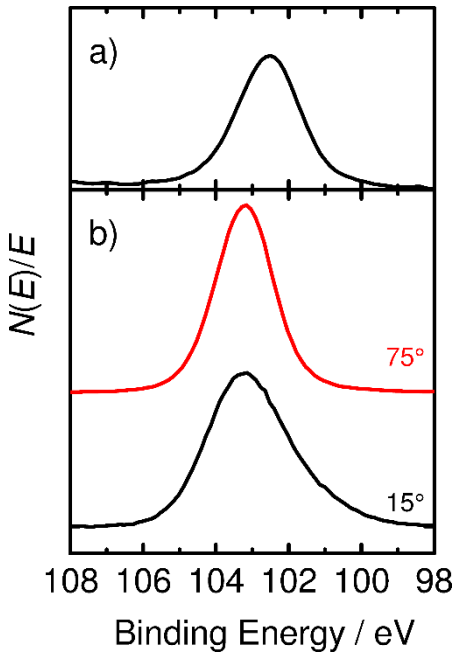

Figure S6. The Si 2p peaks in XPS spectra of the (a) original p(DDA/SQ22) LB films on CaF_2 substrates measured at take-off angle of 45° and (b) photo-oxidized p(DDA/SQ22) LB films on PET substrates measured at take-off angles of 15° and 75°.

Bending Tests for Photo-Oxidized Sample on Flexible PET Substrates

The sample flexibility was tested by the repetitive bending test for LB films with 40 layers. Results show that the resistance increased slightly on the bending cycle with 20 mm in radius, although the bending with 40 mm in radius does not affect the sample resistance. This result demonstrates the durability of the SiO_2 nanofilms with nanoscale thickness.

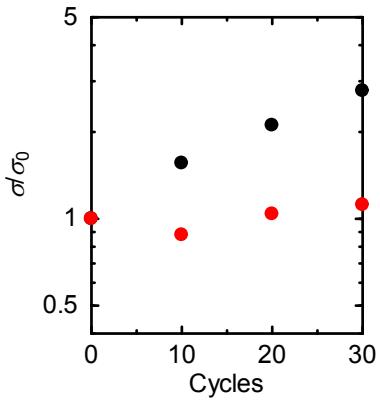

Figure S7. Plot of conductivity after the repetitive bending of the sample to 20 (black) and 40 mm (red) in radius.

Simulation of FT–IR Spectra by Quantum Chemical Calculations

For assignment of the FT–IR spectra, quantum chemical calculations were performed using the density functional theory (DFT) at the DFT/B3LYP level with the 6-31G basis set. For the calculation, the Gaussian 09 program was used.[S1] As a result shown in Figure S8, one peak was simulated at around 1100 cm^{-1} for $SQMe_8$, whereas an additional minor peak was obtained in the low wavenumber region at ca. 1070 cm^{-1} for $SQPh_7Me$ molecule. This spectral feature for $SQPh_7Me$ is similar to that for p(DDA/SQ22), as described in the main text. The strong peak at ca. 1100 cm^{-1} is attributed to the asymmetric vibration of SQ cage, as reported previously. The minor peak is assigned to the coupled vibration of phenyl rings to the SQ cage, as shown in Figure S8.

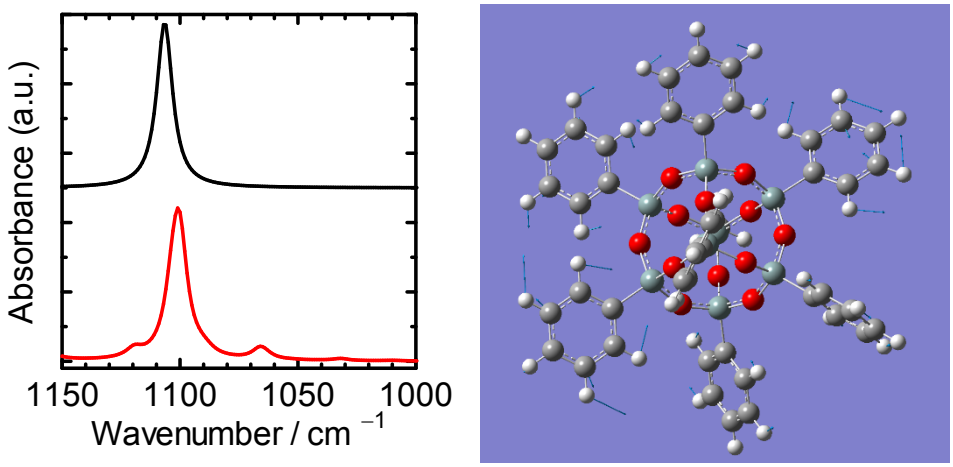

Figure S8. (Left) Simulated IR spectra of $SQMe_8$ (black line) and $SQPh_7Me$ (red line). The half-widths of these spectra are set as 4 cm^{-1}. (Right) The displacement vector in the resonance at 1066 cm^{-1} for $SQPh_7Me$ molecule.

Photo-Oxidization Reaction Mechanism in Deep-UV Light Irradiation

Temporal changes in FT–IR spectra on deep-UV irradiation were estimated for samples with 20 layers and 40 layers using the procedure described in the main text. As a result, each time constant is estimated as shown in Table S1. Furthermore, we performed the deep-UV irradiation in an Ar atmosphere and traced FT–IR spectra. Results show that the time constant is similar to that in ambient condition. These time constants indicate that both deformation of organic moieties and deformation of cage to network structures are controlled by the direct UV light irradiation. However, the final spectra of samples processed in Ar differ slightly from those in ambient conditions, which suggests that the deformation processes is not completed for samples in Ar and some part of cages remain intact. It is particularly interesting that the FT–IR spectra of the sample treated in Ar changed after exposure to ambient condition in the dark for 24 h (Figure S9). This change indicates that deep-UV irradiation without oxygen rearranges the bonds inside of the film to create the network structure. In the surface region, some active species such as radicals remained and such active species react with ambient oxygen to form a network structure.

The temporal change in FT-IR spectra is also evaluated for the sample with 20 layers under low-fluence deep UV irradiation in an Ar atmosphere (Figure S10). As shown in Table S1, the time constants for decomposition of organic moieties is greater than those of n UV–ozone treatment, however, the time constant for deformation of silsesquioxane cage is even longer than that on UV-ozone treatment. This result is consistent to the proposed mechanism for photo-oxidization shown in the main text.

Table S1. Time constants of deformation on deep-UV treatment

Layer Numbers	Atmosphere	Fluence / mW cm^{-2}	τ_{CH} / min	τ_{Ph} / min	τ_{R} / min	τ_{ind} / min	τ_{def} / min
20	Air	300	10	10	20	20	45
40	Air	300	10	10	20	20	45
20	Ar	300	10	10	20	20	45
20	Ar	10	170	160	170	170	>1000

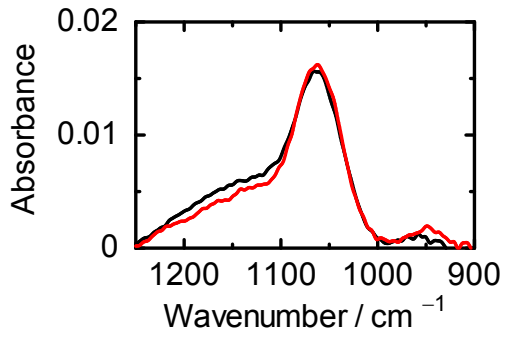

Figure S9. FT–IR spectrum of p(DDA/SQ22) LB films 180 min after deep-UV irradiation in an Ar-filled quartz cuvette (black line). Red line shows the FT–IR spectrum of the sample after exposure to ambient atmosphere for 24 h in the dark.

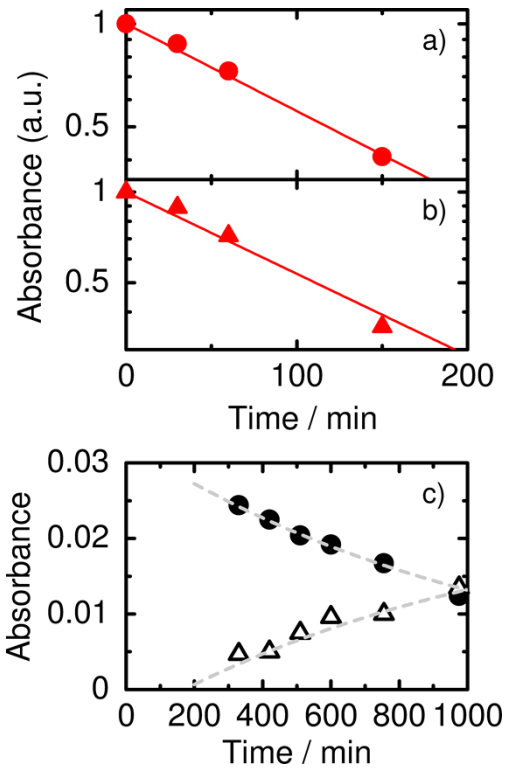

Figure S10. Decay dynamics in FT–IR spectra. (a) and (b) respectively show bands of ν_{CH} in alkyl chains and δ_S in phenyl rings on low-fluence deep UV light irradiation for 20-layer p(DDA/SQ22) LB films. (c) Rise and decay dynamics of cage (closed circles) and network (open triangles) structures estimated by the Gaussian fitting for p(DDA/SQ22) LB films.

References

S1 Gaussian 09, Revision D.01, Frisch, M. J.; Trucks, G. W.; Schlegel, H. B.; Scuseria, G. E.; Robb, M. A.; Cheeseman, J. R.; Scalmani, G.; Barone, V.; Mennucci, B.; Petersson, G. A.; Nakatsuji, H.; Caricato, M.; Li, X.; Hratchian, H. P.; Izmaylov, A. F.; Bloino, J.; Zheng, G.; Sonnenberg, J. L.; Hada, M.; Ehara, M.; Toyota, K.; Fukuda, R.; Hasegawa, J.; Ishida, M.; Nakajima, T.; Honda, Y.; Kitao, O.; Nakai, H.; Vreven, T.; Montgomery, J. A., Jr.; Peralta, J. E.; Ogliaro, F.; Bearpark, M.; Heyd, J. J.; Brothers, E.; Kudin, K. N.; Staroverov, V. N.; Kobayashi, R.; Normand, J.; Raghavachari, K.; Rendell, A.; Burant, J. C.; Iyengar, S. S.; Tomasi, J.; Cossi, M.; Rega, N.; Millam, N. J.; Klene, M.; Knox, J. E.; Cross, J. B.; Bakken, V.; Adamo, C.; Jaramillo, J.; Gomperts, R.; Stratmann, R. E.; Yazyev, O.; Austin, A. J.; Cammi, R.; Pomelli, C.; Ochterski, J. W.; Martin, R. L.; Morokuma, K.; Zakrzewski, V. G.; Voth, G. A.; Salvador, P.; Dannenberg, J. J.; Dapprich, S.; Daniels, A. D.; Farkas, Ö.; Foresman, J. B.; Ortiz, J. V.; Cioslowski, J.; Fox, D. J. Gaussian, Inc., Wallingford CT, **2009**.